International Journal of Nanomedicine

Dovepress
open access to scientific and medical research

Open Access Full Text Article

ORIGINAL RESEARCH

Self-Nanoemulsifying Drug Delivery System of Morin: A New Approach for Combating Acute Alcohol Intoxication

Jiamin Mao[1,2], Xiaoyuan Liu[2], Lie Zhang[1], Yu Chen[2], Shiyu Zhou[2], Yujiao Liu[2], Jing Ye[2], Xiaohong Xu[2], Quan Zhang[1–4]

[1]Department of Neurosurgery, The First Affiliated Hospital of Chengdu Medical College, Chengdu, 610500, People's Republic of China; [2]Sichuan Higher Education Institute Key Laboratory of Structure-Specific Small Molecule Drugs, Institute of Materia Medica, School of Pharmacy, Chengdu Medical College, Chengdu, 610500, People's Republic of China; [3]Development and Regeneration Key Laboratory of Sichuan Province, Department of Anatomy and Histoembryology, Chengdu Medical College, Chengdu, 610500, People's Republic of China; [4]Chengdu Nature's Grace Biological Technology Co., Ltd., Chengdu, 610213, People's Republic of China

Correspondence: Quan Zhang, Email zhangquancdmc@126.com

Purpose: Acute alcohol intoxication (AAI) is a life-threatening medical condition resulting from excessive alcohol consumption. Our research revealed the potential of morin (MOR) in treating AAI. However, MOR's effectiveness against AAI was hindered by its poor solubility in water and low bioavailability. In this study, our aim was to develop a self-nanoemulsifying drug delivery system (SNEDDS) to enhance MOR's solubility and bioavailability, evaluate its anti-AAI effects, and investigate the underlying mechanism.

Methods: The composition of MOR-loaded self-nanoemulsifying drug delivery system (MOR-SNEDDS) was determined by constructing pseudo-ternary phase diagrams, and its formulation proportion was optimized using the Box-Behnken design. Following characterization of MOR-SNEDDS, we investigated its pharmacokinetics and biodistribution in healthy animals. Additionally, we assessed the anti-AAI effects and gastric mucosal protection of MOR-SNEDDS in an AAI mice model, exploring potential mechanisms.

Results: After breaking down into tiny droplets, the optimized mixture of MOR-SNEDDS showed small droplet size on average, even distribution, strong stability, and permeability. Pharmacokinetic studies indicated that MOR-SNEDDS, compared to a MOR suspension, increased the area under the plasma concentration-time curve (AUC_{0-t}) by 10.43 times. Additionally, studies on how drugs move and are distributed in the body showed that MOR-SNEDDS had an advantage in passively targeting the liver. Moreover, in a mouse model for alcohol addiction, MOR not only decreased alcohol levels by boosting the activity of alcohol dehydrogenase (ADH) and aldehyde dehydrogenase (ALDH) in the stomach and liver, which counteracted the loss of righting reflex (LORR), but also reduced alcohol-induced damage to the stomach lining by lowering malondialdehyde (MDA) levels and increasing superoxide dismutase (SOD) levels. Furthermore, MOR-SNEDDS notably amplified these effects.

Conclusion: MOR exhibits significant potential as a new medication for treating AAI, and utilizing MOR-SNEDDS with high oral bioavailability represents a promising new strategy in combating AAI.

Keywords: Morin, self-nanoemulsifying drug delivery system, acute alcohol intoxication, oral bioavailability, alcohol-induced tissue injury

Introduction

Acute alcohol intoxication (AAI) involves initial central nervous system excitation followed by inhibition due to excessive alcohol consumption. Severe intoxication can lead to respiratory failure, ultimately resulting in death. AAI accounts for a significant portion of acute poisonings, constituting approximately 38.81% of all poisoning cases, surpassing poisonings caused by drugs, chemicals, and food.[1] Recent global studies consistently identify AAI as one of the top seven risk factors associated with high mortality rates.[2] Apart from central nervous system depression triggered by alcohol, AAI can cause damage to multiple organs and tissues, including the gastrointestinal tract, liver, and

Received: 5 April 2024
Accepted: 30 August 2024
Published: 18 October 2024

cardiovascular and cerebrovascular systems.[3–5] Therefore, AAI represents a significant public health concern, and its treatment requires addressing both central nervous system depression and alcohol-induced tissue damage.

Naloxone, an opioid receptor antagonist, is commonly used to alleviate the central nervous system depression associated with AAI and promote the rapid recovery of patients.[6] However, this treatment primarily targets relief of central nervous system symptoms and may overlook the harm caused by alcohol and its metabolites to other organs. Metadoxine is another medication employed to manage AAI by speeding up the metabolism of alcohol, but it demonstrates limited direct reversal of alcohol-induced central nervous system depression.[7] Additionally, drugs like the proton pump inhibitor omeprazole, which protect the gastric mucosa, are sometimes used in AAI treatment.[8] However, these drugs are ineffective in counteracting alcoholic coma.[9] Overall, there is an urgent need to develop a new medication for AAI that can address both the alcohol-induced central nervous system depression and the tissue damage caused by alcohol.

Flavonoid compounds like curcumin have been widely recognized for their ability to protect against alcohol-induced damage to various tissues and organs, including the gastric mucosa, liver, and brain.[10] Additionally, dihydromyricetin (DMY), a polyphenolic flavonoid compound, has been identified as a novel medication for treating AAI when administered via intraperitoneal injection.[11] Moreover, our research has shown that orally administered DMY, with high bioavailability facilitated by nano-carriers, effectively protects against AAI-induced central nervous system depression and tissue injury.[12] Inspired by these findings, we have discovered that morin (MOR), which shares a similar chemical structure with DMY, can mitigate AAI-induced alcoholic coma, tissue damage, and mortality in animals. However, MOR's efficacy in treating AAI is limited by its low oral bioavailability, stemming from its poor water solubility and rapid clearance in vivo.[13] Therefore, enhancing the oral bioavailability of MOR is crucial for maximizing its effectiveness in treating AAI.

The self-nanoemulsifying drug delivery system (SNEDDS) is a homogeneous blend of oil phase, emulsifier, and co-emulsifier.[14] Upon oral administration, SNEDDS encounters gastrointestinal fluid and spontaneously forms nano-emulsions due to mild gastrointestinal peristalsis.[15] Serving as a carrier for drugs, SNEDDS not only facilitates the dissolution of the loaded drug in the gastrointestinal tract but also shields the drug encapsulated in the nano-emulsion oil phase from degradation in the gastrointestinal environment. Furthermore, SNEDDS can be absorbed through the intestinal lymphatic pathway, bypassing first-pass metabolism in the liver, thereby enhancing the oral bioavailability of drugs.[16] Consequently, SNEDDS shows promise in overcoming the challenge of oral absorption associated with MOR and enhancing its efficacy in combating AAI. In this study, we developed MOR-loaded SNEDDS, assessed the anti-AAI effectiveness of MOR and MOR-SNEDDS, and investigated the underlying mechanism.

Materials and Methods

Chemistry and Animal

Morin (purity >98%) was procured from Jiangsu Aikon Biopharmaceutical R&D Co., Ltd (Jiangsu, China). Caprylic capric triglyceride (GTCC) was obtained from Xi'an Healthful Biotech Co., Ltd (Xi'an, China). Cremophor EL and Cremophor RH 60 were sourced from Shanghai Aladdin Biochemical Technology Co., Ltd (Shanghai, China). Polyethylene glycol 400 (PEG 400) was purchased from Tianjin Zhiyuan Chemical Reagent Co., Ltd (Tianjin, China). Castor oil, Isopropyl myristate Diethylene glycol monoethyl ether (DGME), Ethyl oleate (EO), Propylene glycol laurate (PGM), Tween-80, and propylene glycol (PG) were obtained from Sichuan Baichun Technology Co., Ltd (Chengdu, China). Cycloheximide (CYC) was provided by Chengdu Huaxia Chemical Reagent Co., Ltd (Chengdu, China). Total superoxide dismutase (T-SOD) and malondialdehyde (MDA) kits were provided by Nanjing Jiancheng Bioengineering Institute (Nanjing, China). All other chemicals were of analytical or high-performance liquid chromatography (HPLC) grade.

Male Sprague-Dawley (SD) rats (180 ~ 220 g) and Kunming mice (18 ~ 22 g) were procured from Chengdu Dashuo Laboratory Animal Co., Ltd (Chengdu, China). All animals were maintained under a 12-hour natural light cycle at environmental conditions of 25±2 °C and 75±5% humidity. Prior to experimentation, the animals underwent a 12-hour fasting period with ad libitum access to water. Animal welfare and study were carried out in strict accordance with the guidelines for the Care and Use of Laboratory Animal, which drafted by the Institutional Animal Care and Use Committee of Chengdu Medical College (Approval NO. CMC-IACUC-2021011).

The schematic diagram for experimental design and procedure is shown in Scheme 1.

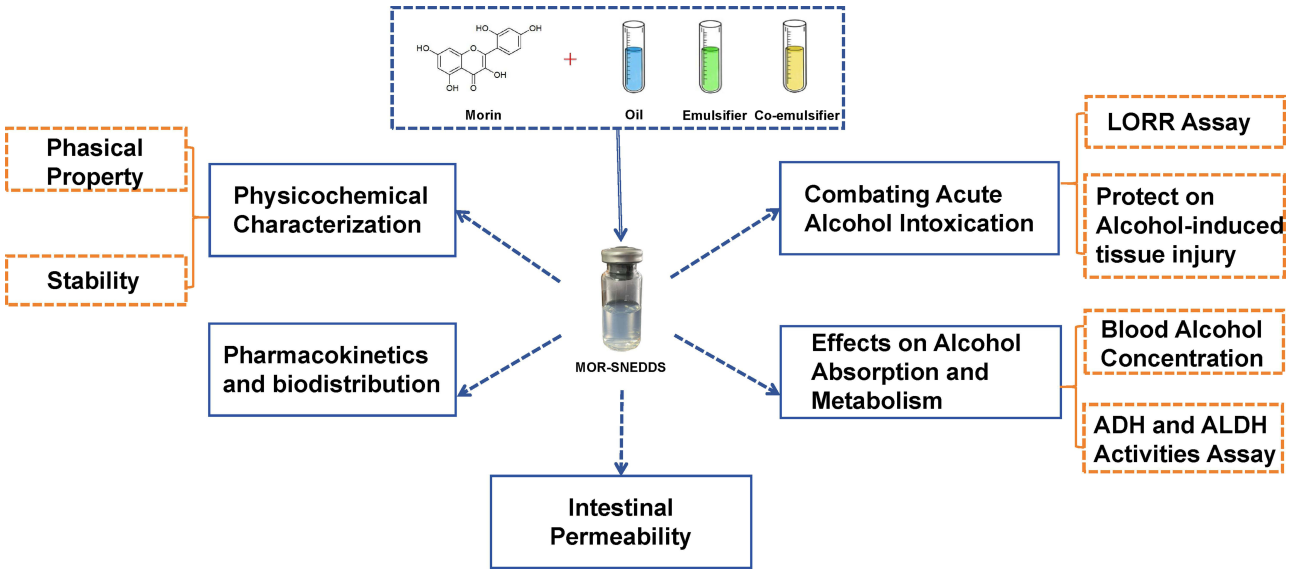

Scheme 1 The experimental design and process.

Quantification of MOR by HPLC

A Shimadzu I-Series (LC-2030) HPLC system equipped with a UV detector was utilized for quantifying MOR. Chromatographic separation was achieved using an Agilent ZORBAX SB-C18 column (150 mm × 4.6 mm, 5 μm) with a mobile phase flow rate of 1.0 mL/min. The mobile phase consisted of 68% A (water containing 0.5% phosphate) and 32% B (methanol). Column temperature was maintained at 30 °C, and detection was performed at a wavelength of 254 nm. The injection volume was 10 μL. The retention time of MOR was 5.205 minutes.

Quantification of MOR by HPLC-MS/MS

Chromatographic separation employed an Agilent XDB-C18 column (4.6 × 50 mm, 1.8 μm) with a mobile phase comprising 55% acetonitrile and 45% distilled water delivered at a flow rate of 0.3 mL/min. Column temperature was set at 30°C, and the injection volume was 1 μL. MOR concentration was determined using a high-performance liquid chromatography/mass spectrometer triple quadrupole system (HPLC-MS/MS, Agilent Technologies, CA, USA). Nitrogen served as the drying gas at a temperature of 350 °C and a flow rate of 11 L/min. The triple-quadrupole mass spectrometer operated in negative electrospray ion source (ESI) mode utilizing multiple reaction monitoring (MRM). The transition of m/z for MOR was 301→151. Optimal MS/MS parameters were set as follows: capillary voltage, 4 kV; atomizing gas pressure, 15 psi; cracking voltage, 100 V; collision energy, 5 V; collision pool acceleration voltage, 7 V. The retention time of MOR was 1.576 minutes.

Determination of Alcohol by GC

Blood alcohol concentration was determined using a flame ionization detector (FID) on an Agilent gas chromatograph (GC) equipped with an automated headspace injection sampler. Separation occurred on an Agilent 19091J-413: HP-5 capillary column (30 m × 320 μm × 0.25 μm). Nitrogen (99.99%) served as the carrier gas at a constant flow rate of 12 mL/min. The heating box and transmission line temperatures were set at 105 °C and 120 °C, respectively. The GC cycle time and equilibrium time were 18 minutes and 10 minutes, respectively. Post-injection temperature was 180 °C, and the column temperature increased from 50 °C to 120 °C over 5 minutes. The FID detector operated at 210 °C. Air flow rate was 400 mL/min, hydrogen gas flow rate was 40 mL/min, and tail blowing gas flow rate was 35 mL/min.

Construction of MOR-SNEDDS

Solubility Study of MOR

The solubility of MOR was determined using the supersaturation method.[17] Excess MOR was added to 1 mL of various lipid media in sealed glass containers. The samples were then kept at 37 °C and stirred at 100 rpm in a thermostatic oscillator for 48 hours. Afterward, the samples were centrifuged at 5054 × g for 10 minutes, and the concentration of MOR in the lipid supernatant was measured by HPLC following moderate dilution with methanol.

Investigation on Emulsifying Capacity of Blank SNEDDS

The mixed emulsifier was prepared by combining an emulsifier and a co-emulsifier, with their masses in a ratio expressed as the Km value. With a fixed Km value of 1, the oil phase and mixed emulsifier were blended in a ratio of 1:5 (w/w) to obtain SNEDDS.[18] One gram of each formulation was dispersed in 500 mL of distilled water at 37 °C using a standard dissolving apparatus. The dissolution paddle was set to rotate at 50 rpm to provide gentle agitation. The in vitro self-emulsifying performance of the formulations was visually evaluated according to the grading system outlined in Table 1.[19] The particle size after emulsification was measured using a Marvin laser particle size meter (MalvernZEN3690, Worcestershire, UK) at 25 °C. Each measurement was repeated three times.

Pseudo-Ternary Phase Diagram

The pseudo-ternary phase diagrams of the formulations graded as A based on the results of the self-emulsifying performance study were generated using the water titration method to determine the range of the self-nanoemulsifying region.[20] The oil phase and mixed emulsifier (with an emulsifier: co-emulsifier ratio of 1:1, w/w) were uniformly blended at weight ratios ranging from 1:9 to 9:1. Under magnetic stirring at 37 °C, each mixture was titrated with distilled water until a transparent self-emulsion with light bluish opalescence was observed. The pseudo-ternary phase diagrams were constructed using Origin 8.0 software, with the three sides of the equilateral triangle representing water, mixed emulsifier, and oil phases, respectively. Each experiment was conducted in triplicate.

Formulation Optimization of MOR-SNEDDS

The MOR-SNEDDS formulation was optimized using a three-factor, three-level Box-Behnken design in Design-Expert 13 software. Employing Box-Behnken design-response surface methodology, with particle size (Y_1, nm) and dispersion (polydispersity index, PDI, Y_2) as response variables, we investigated the effects of the ratio of emulsifier to co-emulsifier (Km, X_1), oil-phase ratio (X_2, %), and the dosage of MOR (X_3, mg) on these variables. The specific independent factors and design levels are detailed in Table 2. The three-dimensional (3D) response surface depicted the fitted polynomial equations. The particle size and PDI of MOR-SNEDDS were determined using a Malvern laser particle size analyzer (MalvernZEN3690, Worcestershire, UK) at 25°C after adequate emulsification in 10 mL of distilled water (sample to distilled water ratio of 1:100, v/v). Measurements were repeated three times.

Preparation of MOR-SNEDDS

The excipients were accurately weighed according to the proportions determined in previous experiments, mixed thoroughly by vortex, and then the blank SNEDDS was obtained. The prescribed amount of MOR was accurately weighed and dispersed in the blank SNEDDS. Finally, MOR-SNEDDS was obtained after complete dissolution by vortex.

Table 1 Visual Evaluation of Self-Emulsifying Performance

Grade	Emulsion Time (minutes)	Dispersibility and Appearance
A	< 1	Rapidly forming nanoemulsion with a clear or bluish appearance
B	< 1	Rapidly forming, slightly less clear emulsion with a bluish white appearance
C	< 2	Fine milky emulsion, similar to milk in appearance
D	> 2	Slow to emulsion, dull, grayish white emulsion having slightly oily appearance
E	> 3	Poor or minimal emulsification with large oil globules present on the surface

Table 2 Levels of Independent Variables in Code and Actual Value in Box-Behnken Design

Independent Variables	Level Used		
	−1	0	1
X_1: Km	1	2	3
X_2: Oil phase ratio (%)	10	20	30
X_3: Drug dosage (mg)	10	20	30

Characterization of MOR-SNEDDS

Particle Size Analysis

The particle size and zeta potential of MOR-SNEDDS were determined using a Malvern laser particle size analyzer (MalvernZEN3690, Worcestershire, UK) at 25°C after adequate emulsification in 10 mL of distilled water (sample to distilled water ratio of 1:100, v/v). Measurements were repeated three times.

Transmission Electron Microscopy Analysis

The morphology of MOR-SNEDDS was observed using a transmission electron microscope (TEM, H-600, Hitachi, Tokyo, Japan). Specifically, after diluting MOR-SNEDDS with pure water, the sample was placed on a copper mesh, negatively stained with 1% phosphotungstic acid, washed with distilled water, and gently dried with filter paper. Subsequently, the sample was observed by TEM and photographed with a digital camera.

Fourier Transform Infrared Spectroscopy Analysis

Fourier transform infrared spectrum (FTIR) analysis of MOR, blank SNEDDS, and MOR-SNEDDS was performed using a NicoletTM iS20 instrument (ThermoFisher, USA). The samples were milled and pressed using potassium bromide tablet technology. The scanning range was 400 to 4000 cm^{-1}.

Entrapment Efficiency (En) and Drug-Loading Percentage (DL)

The encapsulation efficiency (En) and drug loading (DL) of MOR-SNEDDS were determined using a simple and fast centrifugal ultrafiltration technique.[21] This method relies on centrifugal force to separate the free drug, allowing it to pass through the ultrafiltration membrane, while trapping the oil-in-water emulsion. To begin, 200 microliters of MOR-SNEDDS was diluted 100 times with purified water at 37 °C. After gently stirring to create a consistent nanoemulsion, the mixture was transferred to an ultrafiltration tube fitted with a membrane from Labgic Technology Co., Ltd. It was then centrifuged at 4000 × g for 15 minutes. The MOR content was determined using HPLC, and En and DL were calculated accordingly:

$$En\,\% = (1 - \frac{m_{free}}{m_{total}}) \times 100 \tag{1}$$

$$DL(\%) = \frac{m_{drug} - m_{free}}{m_{drug} - m_{free} + m_{excipient}} \times 100 \tag{2}$$

m_{free}: The mass of MOR in the filtrate; m_{drug}: The mass of the initial MOR administration; $m_{excipient}$: Total mass of the initial excipient.

Stability Experiment of MOR-SNEDDS

Stability in Different pH Conditions

The stability of MOR-SNEDDS under various pH conditions resembling the gastrointestinal tract was examined in this study. Simulated gastric fluid (SGF) with a pH of 1.2 was prepared by diluting 16.4 mL of hydrochloric acid with purified water.[22] Simulated intestinal fluids (SIF) with pH values of 6.8 and 7.4 were lightly adjusted according to a method by Fu.[23] Equal volumes of 9.8 mL of SGF and SIF were taken, and 200 μL of MOR-SNEDDS and MOR-DMSO solutions were added to each part. The MOR-DMSO solution was prepared by dissolving 15 mg of pure MOR in 1 mL of dimethyl

sulfoxide (DMSO), yielding a concentration of 15.04 mg/mL. Samples were collected at specific time intervals (0, 0.5, 1, 2, 3, and 4 hours), diluted with methanol, and filtered through a 0.22 μm micropore filter. The concentration of MOR was determined using HPLC, and MOR retention was calculated (n = 3).

Stability in Gastrointestinal and Liver Homogenates

The stability of MOR-SNEDDS in homogenates of the gastrointestinal tract and liver was investigated in this part. Blank stomach, intestine, and liver homogenates (1.9 mL each) were collected, and 100 μL of both MOR-SNEDDS and MOR-DMSO solutions were added (n = 3). Samples (200 μL) were collected at specific time points. Then, 800 μL of methanol was added to precipitate proteins. After centrifugation at 5345 × g for 10 minutes and filtration through a 0.22 μm microporous filter, measurements were conducted following HPLC conditions, and the peak area was recorded to calculate MOR retention.

Pharmacokinetics Study

Twelve healthy male SD rats were randomly divided into two groups: the MOR suspension group and the MOR-SNEDDS group, following a 12-hour fasting period with access to water. Each group received either MOR suspension (MOR was dispersed in 0.5% sodium carboxymethyl cellulose solution) or MOR-SNEDDS at a dose of 100 mg/kg via intragastric administration. Blood samples (0.3 mL) were collected from the inferior orbital venous plexus at 5, 15, 30, 60, 90, 120, 180, 240, and 480 minutes post-administration. The plasma concentration of MOR was analyzed using HPLC-MS/MS.

In vivo Biodistribution

Thirty healthy male SD rats (weighing between 180 and 220 g) were randomly allocated into two groups: the MOR suspension group and the MOR-SNEDDS group, each consisting of 15 rats. For instance, in the MOR suspension group, rats were orally administered MOR suspension at a dose of 100 mg/kg via gavage. Rats were euthanized at 25, 60, and 240 minutes after administration. Subsequently, organs including the heart, liver, spleen, lung, kidney, and brain were promptly excised, weighed, and mixed with normal saline at a 5:1 ratio (tissue weight to saline volume). Tissues were homogenized using a homogenizer with zirconia balls to obtain tissue homogenates. A mixture of 500 μL of methanol and 100 μL of the tissue homogenate was vortexed for 10 minutes. After centrifugation at 12,000 rpm for 10 minutes, the supernatant was collected for analysis.

Intestinal Permeability

The intestinal permeability of MOR-SNEDDS was assessed through a single-pass intestinal perfusion study.[24] In this experiment, eighteen male SD rats were subjected to a 12-hour fast (with access to drinking water) and were randomly divided into three groups: MOR group, MOR-SNEDDS group, and MOR-SNEDDS + CYC group. Rats in the MOR-SNEDDS + CYC group were intraperitoneally injected with a solution of CYC (3 mg/kg) one hour prior to the experiment. All rats received an intraperitoneal injection of a 10% chloral hydrate solution (3 mL/kg) for general anesthesia. Following anesthesia, rats were placed in a supine position, and the abdominal cavity was opened along the midline. The jejunum segment's upper and lower ends were isolated, with the upper end being intubated, washed with normal saline, and emptied, while the lower end was also intubated. A peristaltic pump was connected thereafter. Initially, blank Krebs-Ringers buffer was perfused at 37 °C for 30 minutes at a rate of 0.3 mL/min and then emptied. Subsequently, the test liquid (Krebs-Ringer buffer containing MOR or MOR-SNEDDS) was perfused at a rate of 0.2 mL/min for 30 minutes, initiating the experiment for 15 minutes. After the experiment, the jejunum segments were dissected, and the circumference (c) and length (l) of each segment were measured to compute the radius (r) and volume (v) of the perfused intestinal segment. The MOR content was determined using HPLC, and the absorption rate constant (K_a) and effective permeability coefficient (P_{eff}) were calculated using the following formula:

$$Ka = (1 - \frac{C_{out}\ (m2 - m1)}{C_{in}\ (m3 - m4)}) \frac{Q}{\pi r^2 l} \tag{3}$$

$$Peff = \frac{-Q\ (\frac{C_{out}\ (m2-m1)}{C_{in}\ (m3-m4)})}{2\pi rl} \quad (4)$$

Q represents perfusion velocity (in mL/min); The sum of l and r represents the length (in cm) and the radius (in cm) of cross-section of the irrigated intestine. C_{in} and C_{out} represent the mass concentrations of the enteric inlet and outlet perfusion fluid (in μg/mL), respectively. The value of m_1 and m_2 are the mass of empty collection tube at the outlet of intestinal flow and the mass of collection tube receiving liquid at the outlet after perfusion for a certain time (in grams). Likewise, m_3 and m_4 are the mass of the tube when the perfusion fluid is filled at the enteric flow inlet before perfusion and the remaining fluid and tube mass after a certain period of perfusion (in grams). The density of perfusion fluid does not change much during perfusion, and the default is 1.0 kg/L for both inlet and outlet perfusion fluid.

Effect of MOR-SNEDDS on Alcohol Absorption and Metabolism

Determination of Blood Alcohol Concentration

Fifteen SD rats were evenly distributed into three groups: the model group, MOR suspension group, and MOR-SNEDDS group (n = 5). Rats in the MOR suspension group and MOR-SNEDDS group received MOR suspension and MOR-SNEDDS, respectively, while rats in the model group received an equivalent volume of normal saline. One hour later, all animals were administered 56% alcohol (0.14 mL/10g), and at least 0.3 mL of orbital blood was collected at 5, 60, 120, 240, and 360 minutes, respectively. The blood alcohol concentration was analyzed using GC with headspace injection.

ADH and ALDH Activities Assay

Twenty-four mice were randomly divided into four groups: normal group, model group, MOR suspension group, and MOR-SNEDDS group. Mice in the MOR suspension group and MOR-SNEDDS group were administered MOR suspension and MOR-SNEDDS, respectively, while mice in the normal group and model group received an equal volume of normal saline for one week. On the last day, one hour after drug administration, animals were administered with 56% alcohol (0.15 mL/10g). The mice were euthanized 1 hour later, and the stomach and liver were immediately extracted. The stomach was incised along the greater curvature, and both the stomach and liver were rinsed with normal saline. The activity of ADH and ALDH in each tissue was determined using assay kits.

Combating AAI

LORR Assay

Thirty mice were randomly divided into 3 groups, each comprising 10 mice: the model group, MOR suspension group, and MOR-SNEDDS group. The mice underwent a 12-hour fast without access to water. Mice in the MOR suspension group and MOR-SNEDDS group were administered MOR suspension and MOR-SNEDDS, respectively, while mice in the model group were given an equivalent volume of normal saline. One hour later, all animals were administered 56% alcohol (0.18 mL/10g). Behavioral changes in the mice were observed, with the mice placed in a supine position. The onset time of LORR was recorded if the mice maintained this state for 30 seconds. The onset of LORR was defined from the end of intra-gastric alcohol administration to the beginning of LORR. LORR was considered over when the mice were capable of flipping three times within 30 seconds. The duration of LORR was recorded as the time from the start of LORR until the mice recovered.[25]

Protective Effect on Alcohol-Induced Gastric Mucosal Injury

Mice were randomly divided into four groups, each consisting of 6 mice: the normal group, model group, MOR group, and MOR-SNEDDS group. Mice in the normal group and model group received normal saline (0.2 mL/10 g), while mice in the other two groups were administered MOR suspension and MOR-SNEDDS, respectively. One hour later, mice in the normal group were given normal saline, while mice in the other groups were given absolute ethanol (0.1 mL/10 g). After one hour of induction, the mice were euthanized, and their stomachs were immediately dissected and cut along the greater curvature. The Guth method was utilized to calculate the gastric mucosal injury index, evaluating the degree of gastric mucosa injury.[26] A portion of the injured tissue was fixed with paraformaldehyde for hematoxylin and eosin (HE)

staining and myeloperoxidase (MPO) histochemical analysis. The levels of T-SOD and MDA in each tissue were determined using assay kits.

Statistical Analysis

The results are reported as the mean ± standard deviation (SD). Significant differences were determined by ANOVA followed by Student's *t*-test for multiple comparisons. Differences were considered significant at $P < 0.05$.

Results and Discussion

Solubility Study of MOR

SNEDDS, a drug delivery system composed of an oil phase, emulsifier, and co-emulsifier, serves to enhance the dissolution capacity of insoluble drugs, thereby improving both the rate and extent of drug absorption, leading to enhanced bioavailability. A primary objective in the development of SNEDDS is to optimize the solubility of the compound in the preconcentrate.[27] Hence, this phase of the study entailed screening suitable oil phases, emulsifiers, and co-emulsifiers for the formulation of MOR-SNEDDS through saturation solubility experiments. As depicted in Figure 1A, the saturated solubility of MOR in various lipid media was assessed. Castor oil, GTCC, and PGM were identified as optimal oil phases for MOR dissolution, given their superior solubility. Furthermore, Cremophor RH 60 and Tween-80 were chosen as emulsifiers due to their enhanced ability to dissolve MOR. Additionally, DGME and PEG 400 were employed as co-emulsifiers due to the high solubility of MOR in these agents.

Investigation on Emulsifying Capacity of Blank SNEDDS

SNEDDS disperses to form a fine nanoemulsion under gentle agitation and is administered orally, encountering gastrointestinal fluid in the gastrointestinal lumen. The compatibility of various auxiliary materials in SNEDDS significantly influences the self-emulsification performance of the nanoemulsion.[28] Table 3 illustrates the emulsification performance of blank SNEDDS. Compared to DGME in formulations No. 3, 4, 7, 8, 11, and 12, SNEDDS incorporating PEG 400 as the co-emulsifier exhibits a bluish and transparent appearance upon dispersion and emulsification in distilled water, with a measured polydispersity index (PDI) of less than 0.1. Hence, PEG 400 is selected as the co-emulsifier for SNEDDS.

Pseudo-Ternary Phase Diagram

The pseudo-ternary phase diagram illustrates the self-dispersion capability of SNEDDS to generate thermodynamically stable nanoparticles in the gastrointestinal lumen, providing insights into the phase behavior of SNEDDS with different formulations. The regions of nanoemulsion are delineated on the pseudo-ternary phase diagram, wherein the oil, emulsifier, and co-emulsifier are combined in specific proportions to produce a homogeneous and transparent nanoemulsion.[29] The shaded blue areas in Figure 1B depict nanoemulsion regions corresponding to each formulation. Analysis of the pseudo-ternary phase diagrams reveals that the largest nanoemulsion region aligns with the formulation comprising GTCC, Cremophor RH 60, and PEG 400, indicating superior self-emulsification potential and enhanced thermodynamic stability. Consequently, GTCC was selected as the oil phase, Cremophor RH 60 as the emulsifier, and PEG 400 as the co-emulsifier for constructing MOR-SNEDDS.

Optimization of MOR-SNEDDS Formulation

The droplet size and PDI after emulsification affect the dissolution rate and permeability of the lipid emulsion.[30] Based on preliminary experimental results, the value of Km (X_1) which represents the ratio of the mass of the emulsifier to the co-emulsifier, ratio of oil phase (X_2) and drug dosage (X_3) had significant influence both the particle size (Y_1) and PDI (Y_2), as such, they were taken as the main factors for investigation. Table 4 presents the formulations and response values of MOR-SNEDDS using the 3^3 Box-Behnken design. ANOVA results demonstrated the significance ($P < 0.05$) of both prediction models ($P_{\text{modelY1}} = 0.01$, $P_{\text{modelY2}} = 0.069$), while the lack-of-fit term was not significant ($P_{Y1} = 0.102$, $P_{Y2} = 0.238$, $P > 0.05$), indicating that the regression model effectively describes the changes in response values and exhibits a high degree of fitting with the actual experiment, ensuring reliability. The R^2 values for model Y_1 and Y_2 were 0.9076

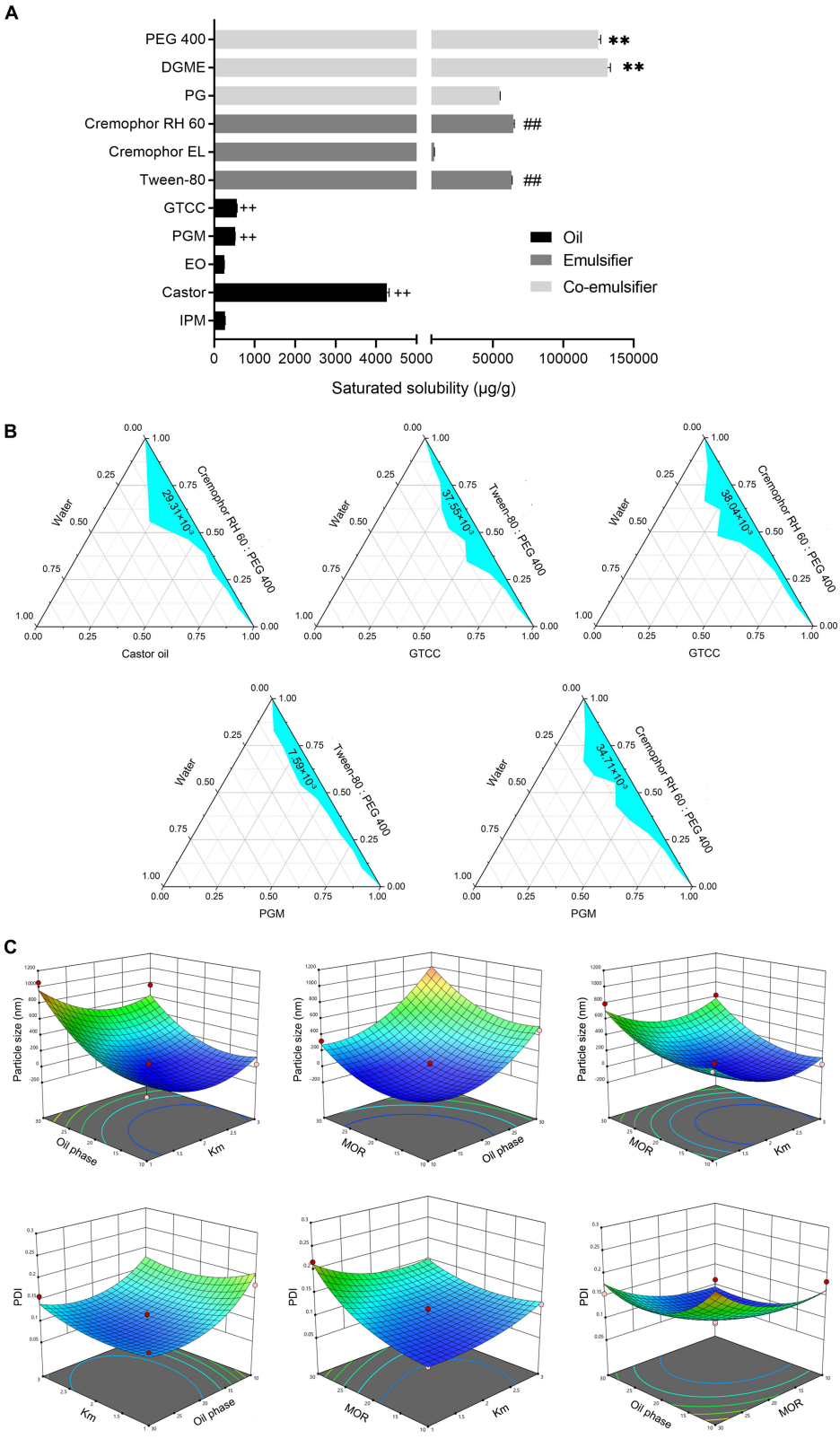

Figure 1 (**A**) Saturated solubility of MOR in different media. (For co-emulsifier, $^{**}P < 0.01$ compared with PG. For emulsifier, $^{\#\#}P < 0.01$ compared with Cremophor EL. For oil phases, $^{++}P < 0.05$ compared with IPM and EO. Each value represents the mean ± SD, $n = 3$). (**B**) Pseudo-ternary phase diagrams of different blank SNEDDS dispersed in water at 37 °C. From left to right and from top to bottom, the composition of the five blank SNEDDS is as follows: Castor oil, Cremophor RH 60, PEG 400; GTCC, Tween-80, PEG 400; with GTCC, Cremophor RH 60, PEG 400; with PGM, Tween-80, PEG 400; PGM, Cremophor RH 60, PEG 400. The blue area represents stable oil-in-water nanoemulsion region. And the values in blue area represent the integration of the sides of oil and mixed emulsifier obtained by mixing emulsifier and co-emulsifier. (**C**) The three-dimensional (3D) response surface representing the influence of the value of Km (X_1), the ratio of oil (X_2, %) and the dosage of MOR (X_3, mg) on particle size (Y_1, nm) and PDI (Y_2) of MOR-SNEDDS.

Table 3 Results of Spontaneous Emulsification of Blank SNEDDS Formulation (n = 3)

Number	Oil Phase	Emulsifier	Co-emulsifier	Emulsifica-tion Grade	Particle Size (nm)	PDI
1	PGM	Tween-80	PEG 400	A	45.3±0.75	0.262±0.01
2	PGM	Tween-80	DGME	C	228.8±4.51	0.277±0.03
3	PGM	Cremophor RH 60	PEG 400	A	35.7±0.70	0.062±0.01
4	PGM	Cremophor RH 60	DGME	B	107.4±1.65	0.293±0.01
5	Castor oil	Tween-80	PEG 400	C	566.7±27.69	0.352±0.09
6	Castor oil	Tween-80	DGME	C	185.9±3.29	0.314±0.05
7	Castor oil	Cremophor RH 60	PEG 400	A	36.3±0.68	0.088±0.01
8	Castor oil	Cremophor RH 60	DGME	B	77.1±2.07	0.228±0.01
9	GTCC	Tween-80	PEG 400	A	55.9±1.10	0.275±0.01
10	GTCC	Tween-80	DGME	C	175.5±3.40	0.204±0.02
11	GTCC	Cremophor RH 60	PEG 400	A	37.4±0.41	0.092±0.01
12	GTCC	Cremophor RH 60	DGME	B	132.2±1.06	0.258±0.01

Table 4 Formulations and Response Values of MOR-SNEDDS Using 3^3 Box-Behnken Design (n = 3)

Number	Independent Variables			Response Variables Values	
	X_1	X_2	X_3	Y_1 (nm)	Y_2
1	0	−1	1	323.8	0.261
2	1	1	0	767.79	0.158
3	0	0	0	33.82	0.114
4	1	0	−1	44.17	0.125
5	0	0	0	40.32	0.099
6	−1	0	1	793.64	0.217
7	−1	1	0	1054.57	0.125
8	1	0	1	623.65	0.148
9	0	0	0	17.23	0.088
10	0	0	0	38.3	0.091
11	0	−1	−1	191.57	0.182
12	0	1	1	834.95	0.155
13	−1	−1	0	72.14	0.182
14	0	0	0	53.43	0.116
15	−1	0	−1	353.7	0.089
16	0	1	−1	468.39	0.085
17	1	−1	0	48.51	0.161

Notes: X_1 (the value of Km), X_2 (the ratio of oil phase, %) and X_3 (the dosage of MOR, mg); Y_1 (particle size, nm) and Y_2 (the value of PDI).

and 0.8961, respectively. Consequently, the fitting model adequately reflected the relationship among the parameters.[31] The fitted equations are provided below:

$$Y1 = 36.62 - 98.74X1 + 311.21X2 + 189.78X3 - 65.79X1X2 + 34.88X1X3 + 58.58X2X3 - 224.12X1^2 + 225.01X2^2 + 193.05X3^2 \quad (5)$$

$$Y2 = -2.29 + 0.0086X1 - 0.2096X2 + 0.2527X3 + 0.0892X1X2 - 0.1806X1X3 + 0.0601X2X3 + 0.1447X1^2 + 0.2848X2^2 + 0.1642X3^2 \quad (6)$$

The 3D response surfaces depicted in Figure 1C elucidate the relationship between independent variables and dependent variables. With an increase in the oil-phase ratio and MOR dosage, the particle size of the nanoemulsion

Table 5 The Predicted Values and Observed Values of the Optimal Formulation (n = 3)

Response	Predicted Values	Observed Values	Relative Error (%)
Y_1	32.79	32.87	0.24
Y_2	0.085	0.089	4.70

gradually increases, while the Km value decreases. Conversely, as the Km value decreases and the MOR dosage increases, the polydispersity index (PDI) of the nanoemulsion gradually increases. According to the mixed interfacial film theory proposed by Sculman, the emulsifier and co-emulsifier act to reduce the water-oil interfacial tension to an ultra-low level, facilitating the spontaneous expansion of the system interface and the formation of nanoemulsions with smaller droplets.[32] Decreasing the oil phase ratio and increasing the emulsifier content enhance drug solubility, elevate emulsification ability, and yield nanoemulsions with smaller particle size and higher stability. The fitting results revealed that the optimal MOR-SNEDDS, with a minimal particle size of 32.8 nm and optimal dispersion (PDI = 0.089), was achieved with a Km value of 1.5, an oil phase ratio of 21%, and MOR dosage of 15 mg. Three parallel experiments were conducted on MOR-SNEDDS using the predicted optimal formulation to validate the model's accuracy. The relative error between the predicted value and the observed value of the response target was less than 5%, confirming the reliability of the optimized formulation (Table 5).

Physicochemical Characterization of MOR-SNEDDS

The constructed MOR-SNEDDS after emulsification exhibited an average particle size of (32.8±1.31) nm (Figure 2A), a polydispersity index (PDI) of (0.089±0.002), and a zeta potential of (−7.2±0.22) mV. A particle size below 100 nm facilitates intestinal lymphatic absorption, thereby bypassing the hepatic portal vein and reducing the first-pass effect.[33] Moreover, a smaller PDI value indicates a more uniform system, which contributes to enhanced stability.[34] TEM images (Figure 2B) revealed that droplets formed post-spontaneous emulsification of MOR-SNEDDS were spherical and uniform in size.

Figure 2C displays the FTIR spectra of pure MOR, SNEDDS without MOR, and MOR-SNEDDS. The FTIR spectra indicate that the peak of the hydroxyl group of MOR is at 3407 cm^{-1}, and the spectral band widens due to the formation of intramolecular or intermolecular hydrogen bonds. The FTIR spectra of MOR-SNEDDS reveal all the peaks of MOR and all the peaks of SNEDDS without any significant change or new peaks. Thus, manifesting the presence of MOR in the SNEDDS and there was no change in the functional groups of the drug and each excipient. Additionally, MOR-SNEDDS demonstrated effective encapsulation with an encapsulation efficiency (En) of 91.71% (Table 6).

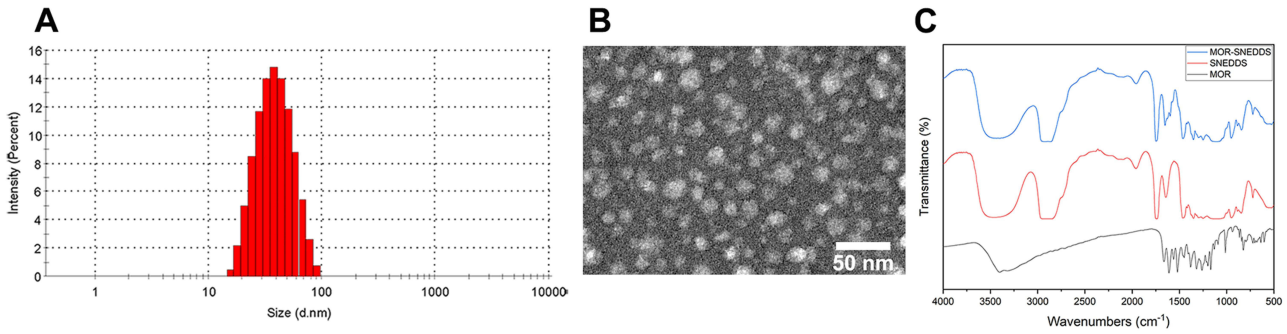

Figure 2 (**A**) Particle size distribution. (**B**) The transmission electron microscopy (TEM) of the self-emulsified MOR-SNEDDS (Bar = 50 nm). (**C**) Fourier transform infrared spectrum (FTIR) spectra of MOR-SNEDDS, the formulation of SNEDDS without MOR, and pure MOR.

Table 6 Results of Encapsulation Efficiency and Drug-Loading Percentage of MOR-SNEDDS (n = 3)

Group	Initial Quantity (mg)	Encapsulation Quantity (mg)	Encapsulation Efficiency (%)	Drug-loading Percentage (%)
1	14.91	13.70	90.99±2.68	1.31±0.08
2	14.93	13.33		
3	14.92	14.02		

Stability of MOR-SNEDDS

The stability of MOR throughout the entire absorption process is pivotal for its oral bioavailability. In this segment of the study, we utilized simulated gastric-intestinal fluid and tissue homogenate (including stomach, intestine, and liver) to replicate the degradation environments of MOR post-oral administration. The stability of MOR and MOR-SNEDDS in an artificially simulated gastric-intestinal fluid environment with varying pH values is illustrated in Figure 3A–C. As depicted in Figure 3A, there is no notable difference in the retention rate of MOR and MOR-SNEDDS over the entire 4-hour incubation period in SGF with a pH of 1.2. The retention rates of MOR and MOR-SNEDDS were 90.46% and 94.96%, respectively, indicating stable presence in SGF. However, in SIF with a pH of 6.5 (Figure 3B), the MOR content gradually declined with increasing incubation time, with retention rates of MOR and MOR-SNEDDS after 4 hours at 51.6% and 79.6%, respectively. Subsequently, after 4 hours of incubation in SIF at pH 7.4 (Figure 3C), MOR experienced rapid degradation with a retention rate of only 37.4%, while MOR-SNEDDS exhibited slower degradation with a retention rate of 69.5%. These findings indicate that the stability of MOR-SNEDDS and MOR is influenced by pH, with both demonstrating good stability under acidic conditions. However, the stability of MOR deteriorates with increasing pH. Overall, the stability of MOR-SNEDDS surpasses that of MOR in an artificially simulated gastric-intestinal fluid environment, suggesting that MOR-SNEDDS prepared in this experiment confers a certain protective effect on MOR.

Drugs administered via the gastrointestinal tract traverse the hepatic portal vein post-absorption by intestinal epithelial cells, subsequently entering the systemic circulation through the liver. However, various metabolizing enzymes in the gastrointestinal tract and liver metabolize drugs within these organs before they reach systemic circulation, thereby reducing the amount of drug reaching systemic circulation; this phenomenon is termed the first-pass effect.[12,35] The

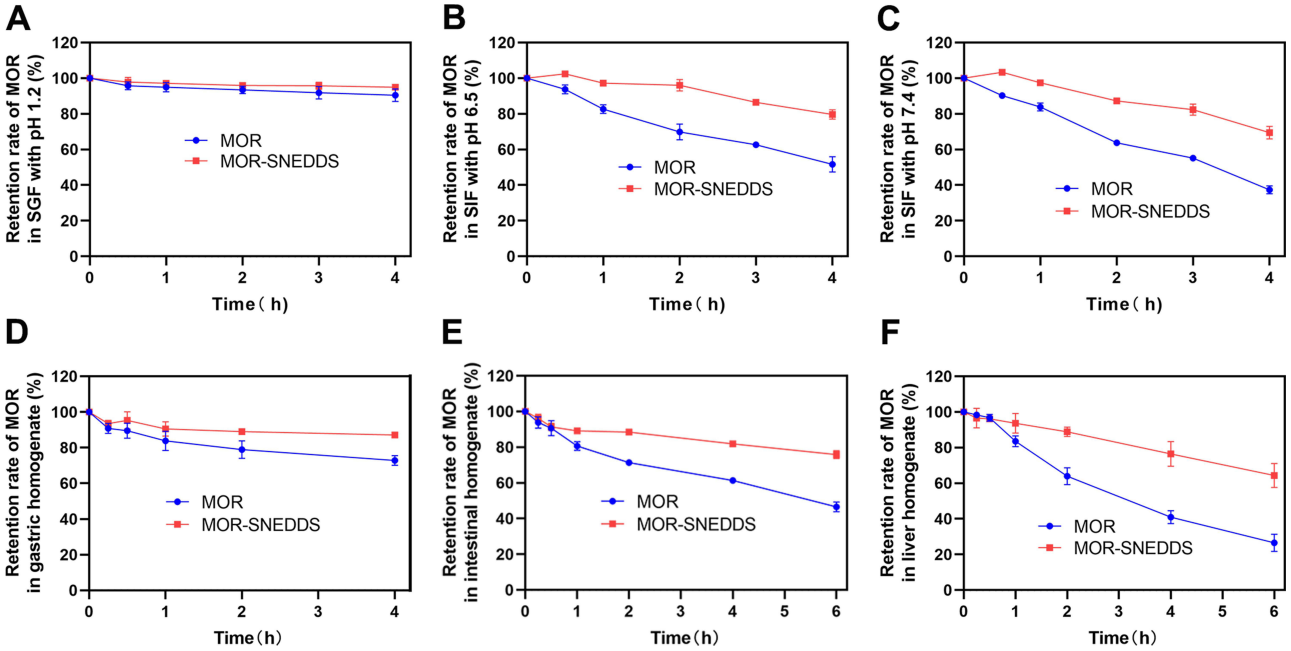

Figure 3 Stability studies of MOR-SNEDDS compared with pure MOR in (**A**) SGF with pH 1.2 and (**B**) SIF with pH 6.5 and (**C**) SIF with pH 7.4, respectively. Stability studies of MOR-SNEDDS compared with pure MOR in (**D**) gastric, (**E**)intestinal and (**F**) liver homogenates. Data are presented as mean ± SD (*n* = 3).

impact of various enzymes in gastrointestinal tract and liver tissue on drugs was investigated by incubating MOR-SNEDDS in tissue homogenates. MOR degraded gradually in gastric homogenate, with MOR content decreasing to approximately 30% after 4 hours of incubation (Figure 3D). In contrast, MOR degraded rapidly within the initial two hours in intestinal homogenate (Figure 3E), with a degradation rate of 53.4% after 6 hours of incubation. These findings suggest that the limited stability of MOR in gastrointestinal homogenates may stem from the actions of various digestive enzymes in the gastrointestinal mucosa and those produced by intestinal flora, resulting in low oral bioavailability of MOR. Owing to the presence of the microsomal drug-metabolizing system in the liver, the MOR content decreased sharply by 73.5% after 6 hours of incubation in liver homogenate (Figure 3F). Conversely, MOR-SNEDDS exhibited greater stability in gastric, intestinal, and liver homogenates compared to pure MOR. The degradation rate of MOR-SNEDDS in gastric homogenate over 4 hours was only 12.9%, and in intestinal homogenate over 6 hours was 24.1%. These results highlight the enhanced stability of MOR-SNEDDS in the gastrointestinal tract compared to pure MOR. This effect may be attributed to the interaction of MOR-SNEDDS with a significant volume of gastric and intestinal fluid upon reaching the gastrointestinal tract, shielding MOR within the water-coated oil emulsion core from digestion and degradation. The oil phase in MOR-SNEDDS potentially acts as a barrier between gastrointestinal digestive enzymes and MOR, thereby indirectly increasing drug absorption in the gastrointestinal tract. Additionally, compared with pure MOR, MOR-SNEDDS can enhance drug stability in liver homogenate to a certain extent (the content of MOR-SNEDDS decreased by 35.6% after 6 hours of incubation in liver homogenate), suggesting that MOR-SNEDDS may mitigate the first-pass effect of the drug and elevate drug concentration in plasma.

Pharmacokinetics and Biodistribution In vivo

Figure 4A depicts the plasma concentration curve of MOR following oral administration of MOR-SNEDDS and MOR suspension in rats. Post-oral administration, the serum concentration of the MOR-SNEDDS group consistently surpassed that of the MOR group across all time points. As evidenced by the pharmacokinetic parameters in Table 7, the maximum blood concentration (C_{max}) for the MOR-SNEDDS group peaked at 4229.10 ng/mL, significantly exceeding that of the MOR group (258.34 ng/mL) ($P < 0.01$). Moreover, the area under the plasma concentration-time curve (AUC_{0-t}) after oral administration of MOR-SNEDDS was 8781.55 ng/L*h, markedly higher than that in the MOR group (768.23 ng/L*h) ($P < 0.01$). Loading the water-insoluble MOR into SNEDDS facilitated complete dissolution of the lipophilic drug in the fatty acids within the formulation. Additionally, the combined action of emulsifier and co-emulsifier expedited rapid self-emulsification when MOR-SNEDDS encountered the water phase in the gastrointestinal tract, forming nano-scale oil-in-water emulsion droplets. This process shielded the drug from enzymatic and chemical hydrolysis in the gastrointestinal tract until absorption by the intestine, consequently enhancing the potential for oral absorption of MOR-SNEDDS.

The results from biodistribution studies of MOR and MOR-SNEDDS revealed notable differences in their accumulation patterns following oral administration. After 25 minutes (Figure 4B), 60 minutes (Figure 4C), and 240 minutes (Figure 4D) of oral MOR suspension administration, MOR accumulation in the liver was 66.09, 132.24, and 41.19 ng/mg, respectively, significantly higher than in other organs, indicating liver as the primary distribution site for MOR. Upon oral administration of MOR-SNEDDS, drug accumulation increased in all organs except the heart compared to the MOR group, with the liver showing the most significant increase ($P < 0.001$). Following 60 minutes of oral MOR-SNEDDS administration, liver accumulation of MOR in rats peaked at 2276.22 ng/mg, a 17.2-fold increase compared to the MOR group ($P < 0.001$). Even after 240 minutes, the MOR-SNEDDS group retained 393.20 ng/mg of MOR in the liver, while most of the MOR group had degraded. Unlike pure MOR, MOR-SNEDDS spontaneously formed nanoemulsion droplets in the gastrointestinal tract upon oral administration, which were absorbed intact by intestinal epithelial cells and subsequently phagocytosed by the reticuloendothelial system upon entering the bloodstream. This passive targeting mechanism led to substantial accumulation in the liver. Consequently, the liver accumulation of MOR-SNEDDS was significantly higher than that of MOR suspension. Additionally, MOR-SNEDDS, as oil-in-water emulsion droplets, exhibited better stability than raw MOR materials, delaying degradation by metabolic enzymes in the liver and prolonging its retention time in the liver. Finally, considering the presence of key enzymes in alcohol metabolism

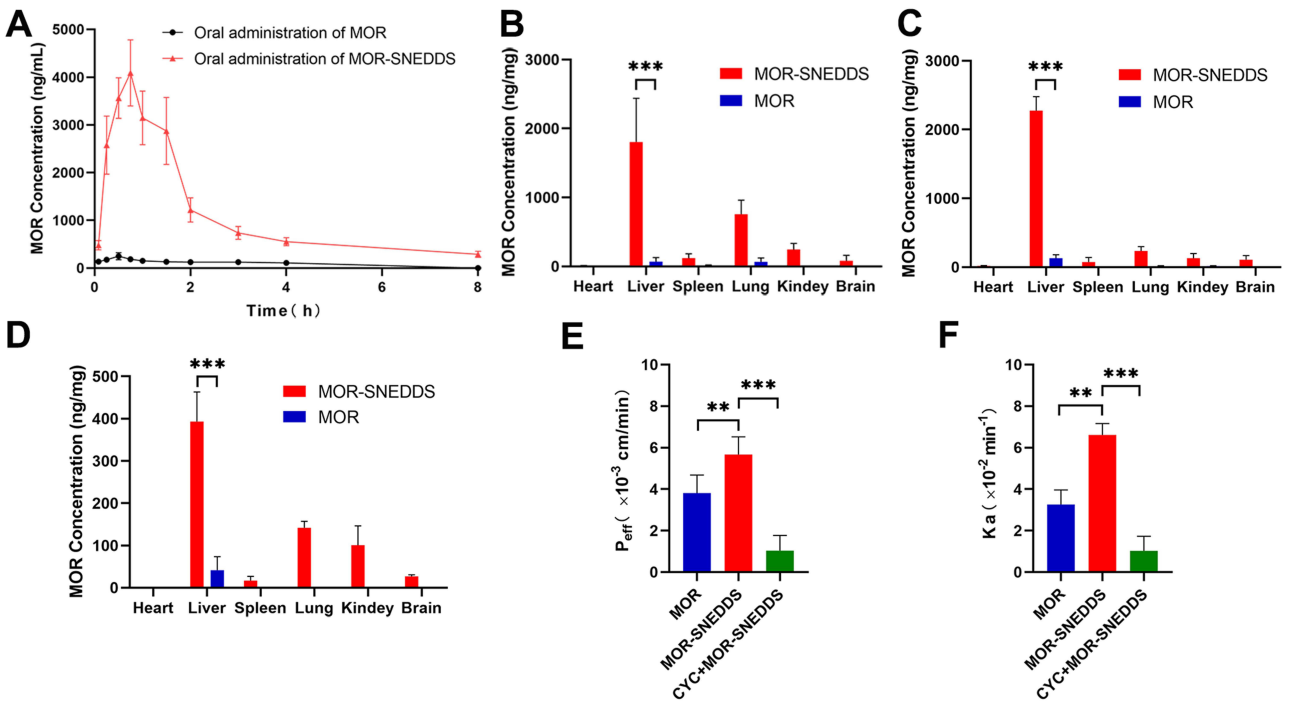

Figure 4 (**A**)The plasma concentration-time curve of MOR in rats after intragastric administration of 100 mg/kg MOR and MOR-SNEDDS, respectively, data are presented as mean ± SD (n = 6). After (**B**) 25 minutes, (**C**) 60 minutes and (**D**) 240 minutes by gavage of MOR and MOR-SNEDDS, the concentration of MOR in the major organs of rats, respectively (***P < 0.001, each value represents the mean ± SD, n = 5). Comparison of (**E**) P_{eff} and (**F**) K_a in jejunum of rats for MOR, MOR-SNEDDS and CYC + MOR-SNEDDS (**P < 0.01, ***P < 0.001, each value represents the mean ± SD, n = 6).

(ADH and ALDH) in the liver, the passive targeting of MOR-SNEDDS to the liver holds importance in maximizing its therapeutic effect on AAI.

Intestinal Permeability

After absorption into the intestinal epithelium, lipophilic molecules can enter the systemic circulation via two distinct pathways: lymphatic transport and portal blood. The absorption of exogenous substances into the lymphatic system through intestinal lymph can occur via three potential pathways: absorption enhancers through the paracellular pathway, M-cells and gut-associated lymphoid tissue, and extracellular pathways linked to the triglyceride core of chylomicrons.[36] Animal lymphatic intubation models and chemical blockade models are commonly used methods for studying drug lymphatic transport. However, the former method often encounters challenges due to the surgical skill required for delicate placement in fragile lymphatic vessels, along with postoperative issues such as cannula detachment, clot formation, and poor lymphatic flow rate.[37] The incorporation of lipophilic molecules into chylomicrons within intestinal epithelial cells is a crucial mechanism for the lymphatic absorption of lipophilic drugs. Therefore, we investigated the

Table 7 Pharmacokinetic Parameters of MOR Suspension and MOR-SNEDDS (100 Mg/Kg) in Rats After Oral Administration (n = 6)

Parameters	MOR Suspension	MOR-SNEDDS
$AUC_{(0-t)}$ (ng/mL*h)	768.234±30.622	8781.549±774.485**
$MRT_{(0-t)}$ (h)	2.463±0.099	2.148±0.126
T_{max} (h)	0.5±0.158	0.875±0.306
C_{max} (ng/mL)	258.345±67.135	4229.104±386.942**

Notes: Data are presented as mean ± SD. **P < 0.01, compared with the MOR suspension group.

MOR-SNEDDS lymphatic transport pathway by chemically blocking the flow of chylomicrons. CYC, a protein synthesis inhibitor, effectively inhibits chylomicron secretion in intestinal cells.[38] Furthermore, the chylomicron flow blockade model offers advantages over other chemical blockade models, including non-toxicity and absence of adverse reactions in experimental animals.[39] The inhibition of chylomicron flow by CYC completely blocked lymphatic absorption components, while non-eluvial absorption components remained unaffected.

The results from rat jejunum unidirectional perfusion revealed significant differences in P_{eff} (Figure 4E) and K_a (Figure 4F) values between MOR and MOR-SNEDDS. Compared to MOR (3.81×10-3 cm/s), MOR-SNEDDS exhibited a notable increase in P_{eff} value (5.67×10-3 cm/s) in the jejunum, representing a 1.49-fold rise ($P < 0.01$). Similarly, the K_a value significantly rose by 2.03 times ($P < 0.01$) for MOR-SNEDDS compared to MOR alone. However, in the rat model with chylomicron flow blockade (CYC+MOR-SNEDDS group), both P_{eff} and K_a values in the jejunum were notably lower than those of the MOR-SNEDDS group ($P < 0.001$). The absorption of MOR-SNEDDS occurred through the intestinal lymphochylomicron pathway as nanoemulsion droplets. Additionally, Cremophor RH 60 present in MOR-SNEDDS acted as a P-glycoprotein inhibitor, mitigating the efflux effect of intestinal epithelial cells on drugs and enhancing the permeability of their cell membranes.[40] This mechanism indirectly facilitated the intestinal absorption of drugs. Overall, MOR-SNEDDS significantly enhances the permeability and absorption rate of MOR in the intestine, bypasses the portal vein, avoids first-pass elimination by the liver, improves the oral bioavailability of the drug, and further enhances its efficacy.

Effect of MOR-SNEDDS on Alcohol Absorption and Metabolism

Determination of Blood Alcohol Concentration

When the body consumes a large amount of alcohol, it enters the bloodstream through the digestive system. Alcohol then spreads throughout the body via the circulatory system, affecting various tissues. Consequently, blood alcohol concentration becomes a critical indicator for assessing how effectively the body eliminates alcohol.[41,42] We measured blood alcohol concentration at different times ranging from 0 to 360 minutes (Figure 5A). In the model group, blood alcohol concentration rose quickly 5 minutes after alcohol intake, reaching its peak at 12.53 mg/mL after 120 minutes, and then began to decline. Compared to the model group, MOR effectively lowered blood alcohol concentration by 40.6% ($P < 0.01$) at 120 minutes and by 18.34% at 360 minutes. Throughout the experiment, rats treated with MOR-SNEDDS had lower blood alcohol concentration than those treated with MOR alone. Particularly at 360 minutes, the blood alcohol concentration in the MOR-SNEDDS group was 50.6% lower than that in the MOR group ($P < 0.05$). These findings demonstrate that MOR effectively reduced alcohol absorption and sped up alcohol metabolism, leading to a decrease in blood alcohol concentration. Importantly, MOR-SNEDDS further improved MOR's ability to enhance alcohol metabolism by increasing MOR's bioavailability.

ADH and ALDH Activities Assay

Alcohol consumption, absorption, and metabolism are key factors determining blood alcohol concentration. Upon intake, alcohol enters the gastrointestinal tract through the mouth, initiating first-pass metabolism (FPM) via alcohol-metabolizing enzymes in the gastric mucosa. This process can decrease alcohol's bioavailability in the body.[43,44] Following circulation, a small portion of alcohol undergoes metabolism and excretion by the kidney and lung, while the liver metabolizes the majority into acetaldehyde through the action of ADH. ADH and ALDH are pivotal in alcohol metabolism. Hence, we evaluated ADH and ALDH activity in gastric and liver tissues of treated mice to elucidate MOR's mechanism in reducing blood alcohol concentration. Our results showed that MOR effectively regulated ADH and ALDH activity levels in the stomach (Figure 5B and C) and ALDH activity levels in liver (Figure 5D and E) of mice ($P < 0.05$). Compared to the normal group, alcohol-induced model group mice exhibited a slight increase in ADH levels in stomach and liver tissues, while ALDH levels decreased. In contrast, MOR treatment effectively increased ADH and ALDH levels in gastric mucosa by 19.8% and 18.8%, respectively. Mice treated with MOR-SNEDDS showed a significant increase in ADH (28.4%, $P < 0.01$) and ALDH (12.4%) levels in gastric mucosa compared to the MOR group. These findings suggest that MOR-SNEDDS enhances MOR's role in up-regulating ADH and ALDH activity in gastric mucosa, accelerating alcohol's FPM and reducing its bioavailability, thereby lowering peak blood alcohol

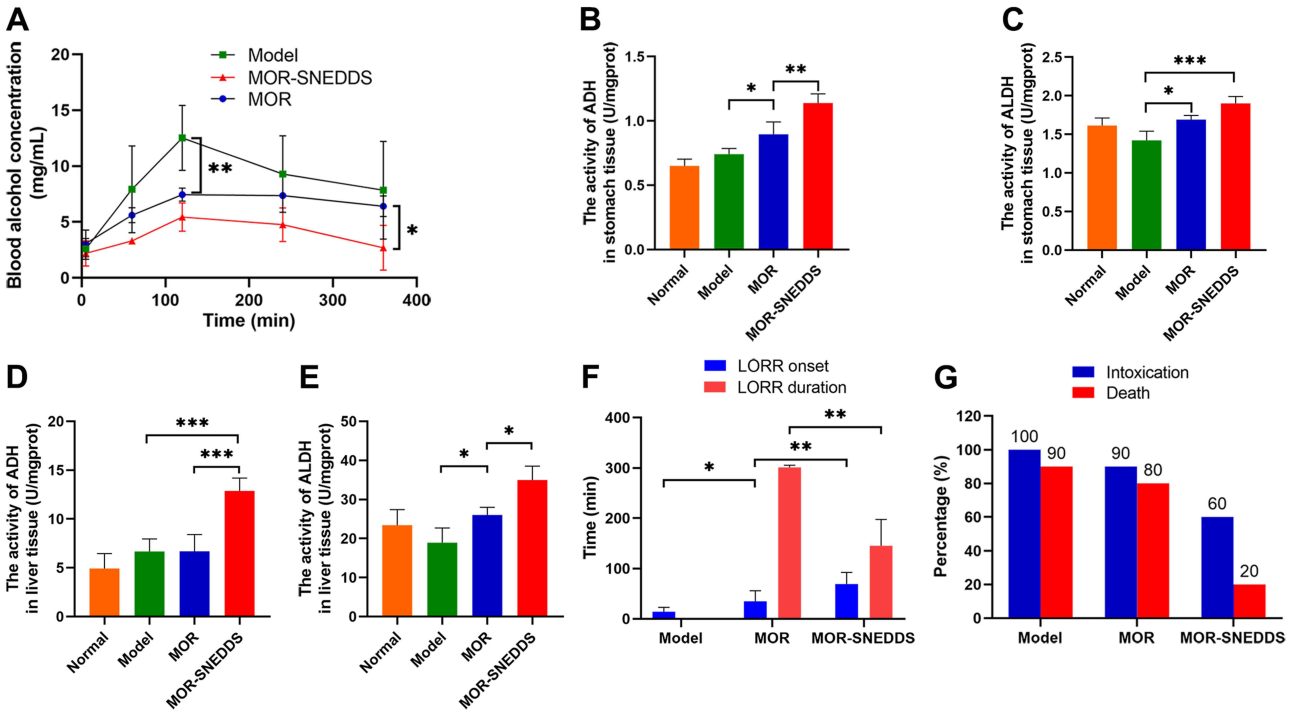

Figure 5 Counteracting effect on alcohol intoxication. (**A**) Blood alcohol concentration-time curve of rats after intragastric administration alcohol. (*P < 0.05, **P < 0.01, the data are presented as mean ± SD, n = 5). The activities of (**B**) ADH and (**C**) ALDH in gastric tissues of mice in each group (*P < 0.05, **P < 0.01, ***P < 0.001, each value represents the mean ± SD, n = 6). The activities of (**D**) ADH and (**E**) ALDH in liver tissue of mice in each group. (*P < 0.05, **P < 0.01, ***P < 0.001, each value represents the mean ± SD, n = 6). (**F**) The results of LORR assay indicate that the MOR treatment could prolong the onset time of alcohol-induced LORR and MOR-SNEDDS significantly enhanced this effect. (All mice in the model group with AAI died, resulting in a LORR duration time value of 0). (*P < 0.05, **P < 0.01, the data are presented as mean ± SD, n = 10). (**G**) The AAI rate and death rate of mice in each group in the LORR experiment (n = 10).

concentration. Moreover, we propose that MOR may protect against gastric mucosal injury induced by high alcohol concentration by expediting alcohol metabolism in the stomach.

MOR increased ALDH activity levels in liver tissues by 37.2% compared with the model group. Moreover, MOR-SNEDDS significantly elevated ADH and ALDH activity levels in liver tissues by 92.27% (P < 0.01) and 34.52% (P < 0.01), respectively, compared to the MOR group. Although there are reports on natural drugs regulating ADH and ALDH levels in the liver to prevent alcoholism,[45,46] the MOR-SNEDDS developed by us offers distinct advantages. In conjunction with the biodistribution study of MOR-SNEDDS, it exhibited a superior passive targeting effect in the liver, significantly enhancing drug accumulation. This intensified the up-regulation effect of MOR on ADH and ALDH activity levels in the liver, facilitating blood alcohol metabolism and reducing blood alcohol concentration. This effect contributes to the anticipated outcome of treating AAI.

Combating on AAI

LORR Assay

We investigated the effects of MOR on alcohol intoxication (LORR) in mice. The normal group of mice exhibited typical behavior, including stable movements and no signs of drowsiness, while those exposed to alcohol displayed symptoms such as irritability, lethargy, slow movement, and loss of coordination. The onset time of LORR in the model group of mice was 14.22 minutes (Figure 5F), with a 100% intoxication rate and a mortality rate of 90% post-intoxication (Figure 5G). In comparison, the MOR group showed a 1.45 times prolongation in the onset time of LORR (Figure 5F) and a slight reduction in intoxication and mortality rates (Figure 5G). Notably, the MOR-SNEDDS group demonstrated a significant 97.7% extension in the onset time of LORR and a reduction of approximately 52% in the duration of LORR (P < 0.01) compared to the MOR group (Figure 5F). Moreover, MOR-SNEDDS effectively decreased the intoxication and post-intoxication mortality rates in mice compared to MOR suspension (Figure 5G). These findings suggest that while MOR showed potential in alleviating the

effects of alcohol on AAI mice, its therapeutic efficacy may be limited due to low oral bioavailability. In contrast, our developed MOR-SNEDDS showed improved efficacy in promoting recovery from alcohol-induced coma and reducing mortality rates in mice.

Protective Effect on Alcohol-Induced Gastric Mucosal Injury

Alcohol exerts significant effects on various organs and tissues, starting from the stomach. When ethanol concentrations exceed 50%, it can trigger several disorders in the gastric mucosa microcirculation, resulting in gastric mucosal congestion, ulcers, and potentially gastric perforation.[47,48] We investigated the protective effects of MOR-SNEDDS against alcohol-induced gastric tissue damage. The extent of gastric mucosal injury in each group of mice is depicted in Figure 6A–C below. Based on the gastric histopathologic map (Figure 6A) and MPO immunohistochemical results (Figure 6B), the gastric tissue of mice in the normal group exhibited a structurally intact gastric lining, well-organized glandular arrangement, and no signs of histopathological damage, bleeding, or inflammation. Conversely, in the model group, the gastric mucosa showed structural irregularities,

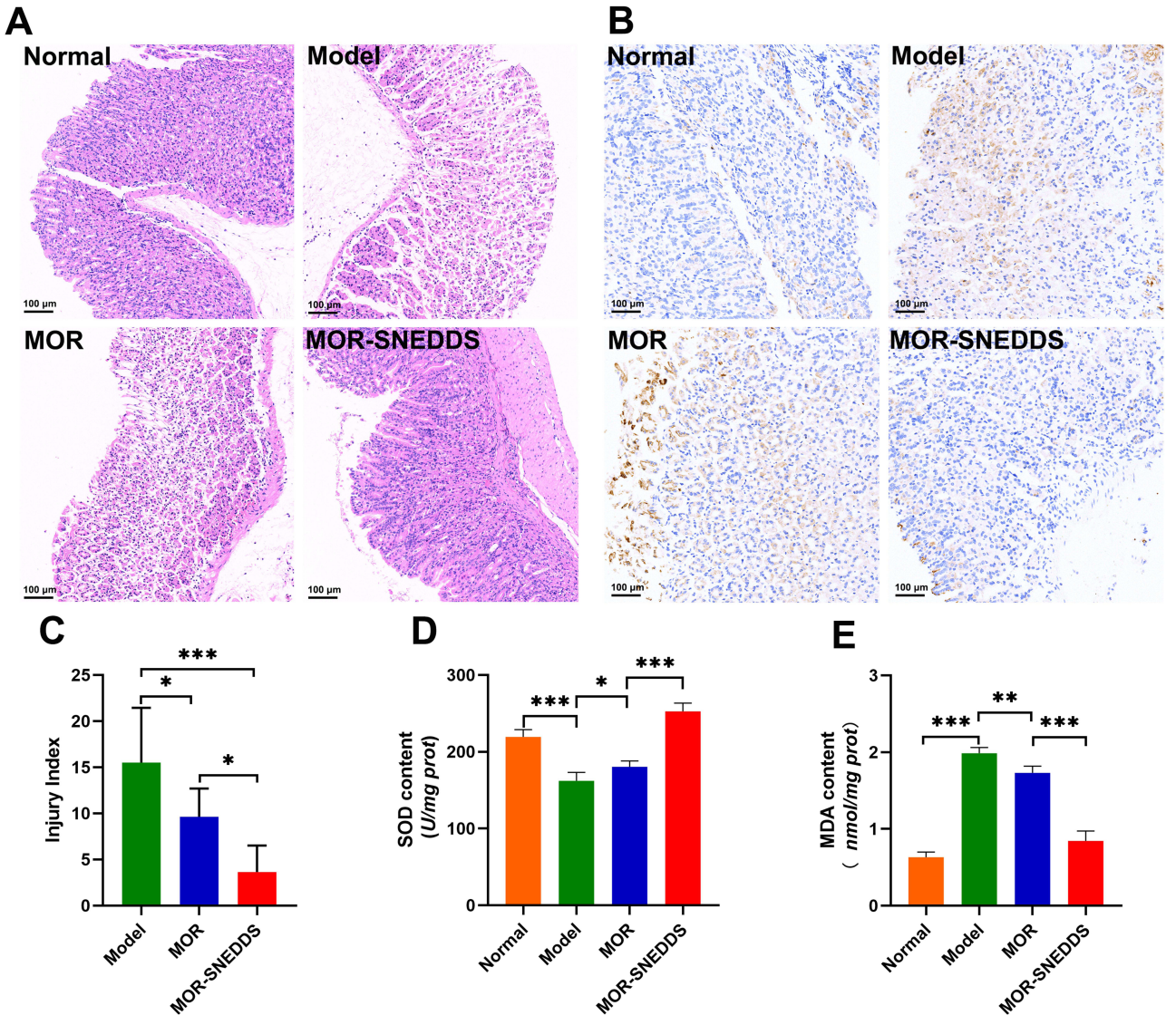

Figure 6 Protective effect on alcohol-induced gastric mucosal injury. (**A**) Pathological morphologic images of gastric mucosa in each group of mice after hematoxylin and eosin staining (Bar = 100 μm). (**B**) Gastric immunohistochemistry of MPO activity in each group, bar = 100 μm. (**C**) In comparison to the model group, the gastric mucosal injury index in the MOR group significantly decreased and MOR-SNEDDS significantly enhanced these effects (*$P < 0.05$, **$P < 0.01$, ***$P < 0.001$, each value represents the mean ± SD, $n = 6$). The (**D**) SOD levels and (**E**) MDA contents in gastric tissues of all groups (*$P < 0.05$, **$P < 0.01$, ***$P < 0.001$, each value represents the mean ± SD, $n = 6$).

disordered cellular arrangement, loss of cell integrity in most cells, and significant neutrophil infiltration. Although gastric tissue injury in the MOR group was slightly reduced compared to the model group, necrosis of main cells persisted, with a substantial separation of apical cells and other adenocytes, leading to disrupted cell columns, and some neutrophil infiltration remained. However, treatment with MOR-SNEDDS resulted in intact gastric tissue with neatly arranged cells and only minimal neutrophil infiltration. The gastric mucosal injury index for mice in the model group (Figure 6C) was 15.5, further confirming the successful establishment of the alcohol-induced gastric mucosal injury model.[49] Compared to the model group, both MOR and MOR-SNEDDS reduced the gastric mucosal injury index by 37.9% ($P < 0.05$) and 76.6% ($P < 0.001$), respectively. Moreover, the gastric mucosal injury index of mice in the MOR-SNEDDS group was significantly lower than that in the MOR group ($P < 0.05$).

While the exact mechanism behind alcohol-induced gastric injury remains unclear, mounting evidence suggests that oxidative stress, inflammatory cytokines, and apoptosis play pivotal roles in the pathogenesis of ethanol-induced gastric ulcers.[50] The expression levels of SOD and MDA in gastric tissue cells serve as indicators of the antioxidant capacity of gastric tissue and the extent of tissue injury.[51,52] As depicted in Figure 6D and E, the model group exhibited significantly reduced SOD activity levels and increased MDA content, indicating the involvement of oxidizing free radicals and lipid peroxides in the pathological process of alcohol-induced gastric mucosal injury, consistent with previous reports in the literature.[53] Compared to the model group, the MOR group showed an 11.2% increase in SOD levels and a 12.8% decrease in MDA levels ($P < 0.05$). Furthermore, treatment with MOR-SNEDDS resulted in a significant 57.5% decrease in MDA expression ($P < 0.001$) and a 40.1% increase in SOD activity ($P < 0.001$) in gastric tissue compared to the MOR group. These findings suggest that MOR-SNEDDS up-regulated SOD expression and down-regulated MDA expression in gastric tissue, thereby reducing oxidative stress reactions and neutrophil accumulation, leading to a more effective protective effect against alcohol-induced gastric tissue injury, which is closely associated with the anti-inflammatory and antioxidative stress properties of MOR.[54]

Conclusion

We found that MOR holds promising potential in mitigating AAI. Additionally, we developed a self-nanoemulsifying drug delivery system (SNEDDS) to enhance MOR's oral absorption and distribution in the liver. Our in vivo investigations demonstrated that MOR moderately alleviated AAI. Moreover, MOR-SNEDDS, with its improved oral absorption and liver distribution, exhibited a notable enhancement in counteracting alcohol-induced central inhibition and tissue damage, thereby reducing AAI-related mortality. In summary, MOR-SNEDDS represents a novel approach for addressing AAI.

Abbreviations

MOR, Morin; SNEDDS, Self-nanoemulsifying drug delivery system; MOR-SNEDDS, Morin-loaded self-nanoemulsifying drug delivery system; GTCC, Caprylic capric triglyceride; PEG 400, Polyethylene glycol 400; IPM, Isopropyl myristate; DGME, Diethylene glycol monoethyl ether; EO, Ethyl oleate; PG, Propylene glycol; PGM, Propylene glycol laurate; CYC, Cycloheximide; ADH, Alcohol dehydrogenase; ALDH, Aldehyde dehydrogenase; LORR, Loss of righting reflex; MPO, Myeloperoxidase; FPM, First-pass metabolism; TEM, Transmission electron microscope; PDI, Polydispersity index; SD, Sprague-Dawley; T-SOD, Total superoxide dismutase; MDA, Malondialdehyde.

Acknowledgments

This work was supported by the financial support from the National Natural Science Foundation of China (No. 81603045), the Sichuan Provincial Natural Science Foundation of China (grant number 2023NSFSC1683), the Engineering Research Center for Pharmaceuticals and Equipments of Sichuan Province Fund (grant number ERCPEF2303) and the Open Fund of Development and Regeneration Key Laboratory of Sichuan Province (grant number SYS22-02).

Disclosure

The authors report no conflicts of interest in this work.

References

1. Jacob A, Wang P. Alcohol intoxication and cognition: implications on mechanisms and therapeutic strategies. *Front Neurosci*. 2020;14:505989. doi:10.3389/fnins.2020.00102
2. Strayer RJ, Friedman BW, Haroz R, et al. Emergency department management of patients with alcohol intoxication, alcohol withdrawal, and alcohol use disorder: a white paper prepared for the American Academy of emergency medicine. *J Emergency Med*. 2023;64(4):517–540. doi:10.1016/j.jemermed.2023.01.010
3. Day AW, Kumamoto CA. Gut microbiome dysbiosis in alcoholism: consequences for health and recovery. *Front Cell Infect Microbiol*. 2022;12:840164. doi:10.3389/fcimb.2022.840164
4. Namachivayam A, Gopalakrishnan AV. A review on molecular mechanism of alcoholic liver disease. *Life Sci*. 2021;274:119328. doi:10.1016/j.lfs.2021.119328
5. Roerecke M. Alcohol's impact on the cardiovascular system. *Nutrients*. 2021;13(10):3419. doi:10.3390/nu13103419
6. Murphy IV CE, Wang RC, Montoy JC, Whittaker E, Raven M. Effect of extended-release naltrexone on alcohol consumption: a systematic review and meta-analysis. *Addiction*. 2022;117(2):271–281. doi:10.1111/add.15572
7. Jiang W, Wei Y, Wen Q, Shi G, Zhao H. Metadoxine inhibits the infiltration of macrophages and neutrophils into liver tissue in acute alcoholic liver injury. *J Chin Pharmaceut Sci*. 2022;31(1). doi:10.5246/jcps.2022.01.005
8. Xie L, Guo Y, Chen Y, et al. A potential drug combination of omeprazole and patchouli alcohol significantly normalizes oxidative stress and inflammatory responses against gastric ulcer in ethanol-induced rat model. *Int Immunopharmacol*. 2020;85:106660. doi:10.1016/j.intimp.2020.106660
9. Mirijello A, Sestito L, Antonelli M, Gasbarrini A, Addolorato G. Identification and management of acute alcohol intoxication. *Eur J Intern Med*. 2023;108:1–8. doi:10.1016/j.ejim.2022.08.013
10. Bao S, Zhang Y, Ye J, et al. Self-assembled micelles enhance the oral delivery of curcumin for the management of alcohol-induced tissue injury. *Pharm Dev Technol*. 2021;26(8):880–889. doi:10.1080/10837450.2021.1950185
11. Shen Y, Lindemeyer AK, Gonzalez C, et al. Dihydromyricetin as a novel anti-alcohol intoxication medication. *J Neurosci*. 2012;32(1):390–401. doi:10.1523/JNEUROSCI.4639-11.2012
12. Ye J, Bao S, Zhao S, et al. Self-assembled micelles improve the oral bioavailability of dihydromyricetin and anti-acute alcoholism activity. *AAPS Pharm Sci Tech*. 2021;22(3):1–11. doi:10.1208/s12249-021-01983-2
13. Li J, Yang Y, Ning E, Peng Y, Zhang J. Mechanisms of poor oral bioavailability of flavonoid Morin in rats: from physicochemical to biopharmaceutical evaluations. *Eur J Pharm Sci*. 2019;128:290–298. doi:10.1016/j.ejps.2018.12.011
14. Niu J, Yuan M, Zhang Z, et al. Hyaluronic acid micelles for promoting the skin permeation and deposition of curcumin. *Int J Nanomed*. 2022;17:4009. doi:10.2147/IJN.S372711
15. Jain S, Dongare K, Nallamothu B, et al. Enhanced stability and oral bioavailability of erlotinib by solid self nano emulsifying drug delivery systems. *Int J Pharm*. 2022;622:121852. doi:10.1016/j.ijpharm.2022.121852
16. Buya AB, Beloqui A, Memvanga PB, Préat V. Self-nano-emulsifying drug-delivery systems: from the development to the current applications and challenges in oral drug delivery. *Pharmaceutics*. 2020;12(12):1194. doi:10.3390/pharmaceutics12121194
17. Jianxian C, Saleem K, Ijaz M, Ur-Rehman M, Murtaza G, Asim MH. Development and in vitro evaluation of gastro-protective aceclofenac-loaded self-emulsifying drug delivery system. *Int J Nanomed*. 2020;Volume 15:5217–5226. doi:10.2147/IJN.S250242
18. Krishna VM, Kumar VB, Dudhipala N. In-situ intestinal absorption and pharmacokinetic investigations of carvedilol loaded supersaturated self-emulsifying drug system. *Pharmaceut nanotechnol*. 2020;8(3):207–224. doi:10.2174/2211738508666200517121637
19. Liu C, Chen L, Hu Y, et al. Self-microemulsifying drug delivery system for improved oral delivery and hypnotic efficacy of ferulic acid. *Int J Nanomed*. 2020;Volume 15:2059–2070. doi:10.2147/IJN.S240449
20. Dou Y, Zhou J, Wang T, et al. Self-nanoemulsifying drug delivery system of bruceine D: a new approach for anti-ulcerative colitis. *Int J Nanomed*. 2018;Volume 13:5887–5907. doi:10.2147/IJN.S174146
21. Wu J, Cui Y, Yu B, et al. A simple way to simultaneously release the interface stress and realize the inner encapsulation for highly efficient and stable perovskite solar cells. *Adv Funct Mater*. 2019;29(49):1905336. doi:10.1002/adfm.201905336
22. Axson JL, Stark DI, Bondy AL, et al. Rapid kinetics of size and pH-dependent dissolution and aggregation of silver nanoparticles in simulated gastric fluid. *J Phys Chem C*. 2015;119(35):20632–20641. doi:10.1021/acs.jpcc.5b03634
23. Wang L, Wang Y, Xu M, et al. Enhanced hepatic cytotoxicity of chemically transformed polystyrene microplastics by simulated gastric fluid. *J Hazard Mater*. 2021;410:124536. doi:10.1016/j.jhazmat.2020.124536
24. Ren Q, Zhao S, Zhu Y, et al. Supramolecular aggregates of myricetin improve its bioavailability and its role in counteracting alcoholism. *J Drug Deliv Sci Technol*. 2022;74:103515. doi:10.1016/j.jddst.2022.103515
25. Egervari G, Siciliano CA, Whiteley EL, Ron D. Alcohol and the brain: from genes to circuits. *Trends Neurosci*. 2021;44(12):1004–1015. doi:10.1016/j.tins.2021.09.006
26. Guth PH. Pathogenesis of gastric mucosal injury. *Annu Rev Med*. 1982;33(1):183–196. doi:10.1146/annurev.me.33.020182.001151
27. Eltobshi AA, Mohamed EA, Abdelghani GM, Nouh AT. Self-nanoemulsifying drug-delivery systems for potentiated anti-inflammatory activity of diacerein. *Int J Nanomed*. 2018;Volume 13:6585–6602. doi:10.2147/IJN.S178819
28. Salawi A. Self-emulsifying drug delivery systems: a novel approach to deliver drugs. *Drug Deliv*. 2022;29(1):1811–1823. doi:10.1080/10717544.2022.2083724
29. Van Staden D, Du Plessis J, Viljoen J. Development of a self-emulsifying drug delivery system for optimized topical delivery of clofazimine. *Pharmaceutics*. 2020;12(6):523. doi:10.3390/pharmaceutics12060523
30. Tran P, Park J. Recent trends of self-emulsifying drug delivery system for enhancing the oral bioavailability of poorly water-soluble drugs. *J Pharm Investig*. 2021;51(4):439–463. doi:10.1007/s40005-021-00516-0
31. Wyantuti S, Fadhilatunnisa B, Fauzia RP, Qi J, Rahmani AA, Bahti HH. Response surface methodology box-behnken design to optimise the hydrothermal synthesis of gadolinium nanoparticles. *Chin J Anal Chem*. 2023;51(10):100316. doi:10.1016/j.cjac.2023.100316
32. Schulman JH, Stoeckenius W, Prince LM. Mechanism of formation and structure of micro emulsions by electron microscopy. *J Phys Chem*. 1959;63(10):1677–1680. doi:10.1021/j150580a027

33. Mahmoudian M, Valizadeh H, Löbenberg R, Zakeri-Milani P. Enhancement of the intestinal absorption of bortezomib by self-nanoemulsifying drug delivery system. *Pharm Dev Technol*. 2020;25(3):351–358. doi:10.1080/10837450.2019.1699109
34. Teng F, He M, Xu J, et al. Effect of ultrasonication on the stability and storage of a soy protein isolate-phosphatidylcholine nanoemulsions. *Sci Rep*. 2020;10(1):14010. doi:10.1038/s41598-020-70462-8
35. Zhao C, Ying Z, Hao D, Zhang W, Ying X, Yang G. Investigating the bioavailabilities of olerciamide A via the rat's hepatic, gastric and intestinal first-pass effect models. *Biopharm Drug Dispos*. 2019;40(3–4):112–120. doi:10.1002/bdd.2175
36. Franco V, Gershkovich P, Perucca E, Bialer M. The interplay between liver first-pass effect and lymphatic absorption of cannabidiol and its implications for cannabidiol oral formulations. *Clin Pharmacokinet*. 2020;59(12):1493–1500. doi:10.1007/s40262-020-00931-w
37. Verma R, Kaushik D, Kumari B, Khatkar A. Lymphatic transport of lipid-based drug delivery system. *A Comprehensive Text Book Self-Emulsifying Drug Delivery Sys*. 2021;95. doi:10.2174/9789814998000121010008
38. Yin K, Tong M, Suttapitugsakul S, Xu S, Wu R. Global quantification of newly synthesized proteins reveals cell type-and inhibitor-specific effects on protein synthesis inhibition. *PNAS nexus*. 2023;2(6):d168. doi:10.1093/pnasnexus/pgad168
39. Ryšánek P, Grus T, Lukáč P, et al. Validity of cycloheximide chylomicron flow blocking method for the evaluation of lymphatic transport of drugs. *Br J Pharmacol*. 2021;178(23):4663–4674. doi:10.1111/bph.15644
40. Mirzaeei S, Tahmasebi N, Islambulchilar Z. Optimization of a self-microemulsifying drug delivery system for oral administration of the lipophilic drug, resveratrol: enhanced intestinal permeability in rat. *Adv Pharm Bull*. 2023;13(3):521. doi:10.34172/apb.2023.054
41. Zhao W, Hu Y, Li C, et al. Transplantation of fecal microbiota from patients with alcoholism induces anxiety/depression behaviors and decreases brain mGluR1/PKC ε levels in mouse. *Biofactors*. 2020;46(1):38–54. doi:10.1002/biof.1567
42. Li J, Wang H, Li M, et al. Effect of alcohol use disorders and alcohol intake on the risk of subsequent depressive symptoms: a systematic review and meta-analysis of cohort studies. *Addiction*. 2020;115(7):1224–1243. doi:10.1111/add.14935
43. Jones AW. Pharmacokinetics of ethanol: a primer for forensic practitioners. *Alcohol, Drugs, Impaired Driving*. 2020;15:275–346.
44. Jiang Y, Zhang T, Kusumanchi P, Han S, Yang Z, Liangpunsakul S. Alcohol metabolizing enzymes, microsomal ethanol oxidizing system, cytochrome P450 2E1, catalase, and aldehyde dehydrogenase in alcohol-associated liver disease. *Biomedicines*. 2020;8(3):50. doi:10.3390/biomedicines8030050
45. Zhang Z, Li S, Jiang J, et al. Preventive effects of Flos Perariae (Gehua) water extract and its active ingredient puerarin in rodent alcoholism models. *Chin Med*. 2010;26:5:36. doi: 10.1186/1749-8546-5-36
46. Sung C, Kim S, Oh C, et al. Taraxerone enhances alcohol oxidation via increases of alcohol dehyderogenase (ADH) and acetaldehyde dehydrogenase (ALDH) activities and gene expressions. *Food Chem Toxicol*. 2012;50(7):2508–2514. doi: 10.1016/j.fct.2012.04.031
47. Ren S, Wei Y, Wang R, et al. Rutaecarpine ameliorates ethanol-induced gastric mucosal injury in mice by modulating genes related to inflammation, oxidative stress and apoptosis. *Front Pharmacol*. 2020;11:600295. doi:10.3389/fphar.2020.600295
48. Chen X, Zhao Y, Liu K, et al. Lycopene aggravates acute gastric injury induced by ethanol. *Front Nutr*. 2021;8:697879. doi:10.3389/fnut.2021.697879
49. Duan Z, Yu S, Wang S, et al. Protective effects of piperine on ethanol-induced gastric mucosa injury by oxidative stress inhibition. *Nutrients*. 2022;14(22):4744. doi:10.3390/nu14224744
50. Chen W, Wu D, Jin Y, et al. Pre-protective effect of polysaccharides purified from Hericium erinaceus against ethanol-induced gastric mucosal injury in rats. *Int J Biol Macromol*. 2020;159:948–956. doi:10.1016/j.ijbiomac.2020.05.163
51. Kolgazi M, Cilingir S, Yilmaz O, et al. Caffeic acid attenuates gastric mucosal damage induced by ethanol in rats via nitric oxide modulation. *Chem Biol Interact*. 2021;334:109351. doi:10.1016/j.cbi.2020.109351
52. Zou Y, Cui X, Xiang Q, et al. Protective effect of against ethanol-induced gastric ulcer and its mechanism. *Med Sci*. 2021;50(5):561–567. doi:10.3724/zdxbyxb-2021-0055
53. Liu Y, Sui D, Fu W, et al. Protective effects of polysaccharides from panax ginseng on acute gastric ulcers induced by ethanol in rats. *Food Funct*. 2021;12(6):2741–2749. doi:10.1039/D0FO02947E
54. Shyma RL, Mini S. Neuroprotective effect of Morin via TrkB/Akt pathway against diabetes mediated oxidative stress and apoptosis in neuronal cells. *Toxicol Mech Methods*. 2022;32(9):695–704. doi:10.1080/15376516.2022.2065225